

# Trajectory Tracking Near Small Bodies Using Only Attitude Control

Xiangyu Li\*

*Beijing Institute of Technology, 100081 Beijing, People's Republic of China*

Rakesh R. Warier<sup>†</sup> and Amit K. Sanyal<sup>‡</sup>

*Syracuse University, Syracuse, New York 13244*

and

Dong Qiao<sup>§</sup>

*Beijing Institute of Technology, 100081 Beijing, People's Republic of China*

DOI: 10.2514/1.G003653

**Gravitational orbit–attitude coupling shows a noticeable influence on the motion of a rigid spacecraft in close proximity to small solar system bodies. The gravity gradient moment changes the attitude of the spacecraft, which in turn alters the total gravity force on the spacecraft and has an impact on the orbital motion. In this paper, the polyhedron model of small bodies is adopted and a distributed point-mass model of the spacecraft is developed to reflect this coupling phenomenon more accurately. In particular, taking advantage of the gravitational orbit–attitude coupling, a trajectory tracking scheme for a rigid body using only attitude control is proposed. By changing the attitude of the spacecraft, the gravitational orbit–attitude coupling generates a control force to make the spacecraft track the reference trajectory. This reference trajectory is generated based on a point-mass model. Simulation results in landing and orbiting around asteroid Bennu show the feasibility of this tracking approach. A significant improvement is seen for the coupling-based controlled trajectory over natural motions. The tracking scheme reduces the frequency of orbit control maneuvers and provides a redundant control in the event of thruster failures. This approach can be used as a reference for future small-body missions.**

## Nomenclature

$\{\mathbb{B}\}^a$	= asteroid-fixed frame
$\{\mathbb{B}\}^s$	= spacecraft body-fixed frame
$e$	= position error in the asteroid-fixed frame
$F$	= force due to gravity on the spacecraft in the asteroid-fixed frame
$G$	= gravity constant
$h$	= integration step size
$h_c$	= attitude control step size
$\{\mathbb{I}\}^a$	= asteroid-centered inertial frame
$J_a$	= moment of inertia of the asteroid
$J_s$	= moment of inertia of the spacecraft
$M$	= gravity gradient moment on the spacecraft in the body-fixed frame
$m$	= total mass of the spacecraft
$Q$	= attitude tracking error
$R$	= rotation matrix from the body-fixed frame of the spacecraft to the asteroid-fixed frame
$R_a$	= rotation matrix from the asteroid-fixed frame to the inertial frame
$R_s$	= rotation matrix from the body-fixed frame of the spacecraft to the inertial frame
$u$	= control acceleration in the asteroid-fixed frame
$V$	= translational velocity vector of the spacecraft in the asteroid-fixed frame

$v$	= translational velocity vector of the spacecraft in the inertial frame
$X$	= position vector of the spacecraft in the asteroid-fixed frame
$x$	= position vector of the spacecraft in the inertial frame
$\Gamma$	= linear momentum of the spacecraft in the asteroid-fixed frame
$\nu$	= translational velocity vector of the spacecraft in the body-fixed frame
$\Pi_s$	= angular momentum of the spacecraft in the body-fixed frame
$\sigma$	= density of the asteroid
$\tau_c$	= control torque on the spacecraft
$\Phi$	= exponential coordinate of attitude
$\phi_c$	= control force on the spacecraft
$\Omega$	= angular velocity vector of the spacecraft in asteroid-fixed frame
$\Omega_a$	= angular velocity vector of the asteroid in the asteroid-fixed frame
$\Omega_s$	= angular velocity vector of the spacecraft in the body-fixed frame of the spacecraft

## I. Introduction

**R**ECENT interest in small solar system bodies, such as asteroids and comets, has led to several spacecraft missions to these bodies. These small bodies are considered as “remnant material” from the formation of the solar system that may contain information on the formation of Earth, the evolution of the solar system, and even origins of life on Earth [1]. Moreover, the abundance of many minerals on these small bodies has led to mission concepts for resource utilization and mining operations targeting these bodies. Several missions have been proposed to explore asteroids and comets. One of the key issues that these mission designs need to address is the dynamics and control of spacecraft in the proximity of these small bodies.

Missions such as NEAR Shoemaker [2], Hayabusa [3], and Rosetta [4,5] have shown that the dynamics environment near small bodies is complex and chaotic. The strong perturbation caused by irregular shape, nonhomogeneous mass distribution, and nonuniform

Received 11 March 2018; revision received 15 June 2018; accepted for publication 18 June 2018; published online 27 September 2018. Copyright © 2018 by the American Institute of Aeronautics and Astronautics, Inc. All rights reserved. All requests for copying and permission to reprint should be submitted to CCC at [www.copyright.com](http://www.copyright.com); employ the ISSN 0731-5090 (print) or 1533-3884 (online) to initiate your request. See also AIAA Rights and Permissions [www.aiaa.org/randp](http://www.aiaa.org/randp).

\*Ph.D. Candidate, School of Aerospace Engineering; [lixiangyu@bit.edu.cn](mailto:lixiangyu@bit.edu.cn).  
<sup>†</sup>Postdoctoral Fellow, Department of Mechanical and Aerospace Engineering; [rwarier@syr.edu](mailto:rwarier@syr.edu).

<sup>‡</sup>Associate Professor, Department of Mechanical and Aerospace Engineering; [aksanyal@syr.edu](mailto:aksanyal@syr.edu) (Corresponding Author).

<sup>§</sup>Professor, School of Aerospace Engineering; Key Laboratory of Dynamics and Control of Flight Vehicle; [qiaodong@bit.edu.cn](mailto:qiaodong@bit.edu.cn).

rotation of small bodies makes proximity operations around these bodies very different from those around planets and large moons. Several studies have dealt with this issue in the past. Natural dynamics such as equilibrium points [6–9], (quasi-)periodic orbits [10,11], retrograde orbits [12], and terminator orbits [13,14] have been investigated, mostly based on a point-mass model of the spacecraft. Controlled motion such as hovering [15,16] and landing [17] has been proposed. Those studies have helped improve our understanding of the dynamic environment in the vicinity of small bodies and facilitated mission design.

Besides the strong perturbation to orbital motion due to irregularities in shape and mass distribution, another key problem in motion near small bodies is the coupling between the translational and rotational motions of a spacecraft caused by the so-called gravitational orbit–attitude coupling, which is induced by the weak gravity of the small body acting on various parts of the spacecraft body. The gravity gradient moment on the spacecraft changes the attitude of the spacecraft, which in turn alters the total gravity force on the spacecraft and has an impact on the orbital motion. The effect of the gravitational coupling depends on the spacecraft mass distribution, orientation, and distance to the small body. Gravitational orbit–attitude coupling and related control problems have been investigated since the 1960s [18]. Sincarsin and Hughes described the effect of orbit–attitude coupling by the parameter  $\varepsilon = (r/R_c)$ , where  $r$  is the characteristic spacecraft size and  $R_c$  is the radius of the orbit [19]. For planetary missions such as those in low Earth orbit, the radius of an orbit is much larger than the size of a spacecraft. In this case, the coupling effect is weak. However, for the small-body proximity missions, the radius of orbit is much smaller, leading to a large value of  $\varepsilon$ ; and the effect due to the gravitational orbit–attitude coupling cannot be ignored. Therefore, orbit–attitude coupling should be considered for accurate mission designs near small bodies [20]. Lian et al. discussed the orbit–attitude coupling effects and the controllability of spacecraft systems in a central gravitational field [21]. Sanyal studied the coupled dynamics and control problem in the context of a multibody system [22]. The coupled dynamics of the spacecraft with an asteroid was mentioned by Scheeres in the design of the large gravity-tractor [23]. Then, Wang and Xu investigated the perturbation of the satellites' inertia integrals around a spheroid planet and indicated that the coupling was severe in the case of a large spacecraft around a small asteroid [24]. The impact of orbit–attitude coupling for spacecraft in a spherical harmonic gravity field was investigated, and a relative motion estimation scheme was proposed by Misra et al. [25]. Based on a similar model, Wang and Xu analyzed the equilibria state of coupling motion [20,26]. Kikuchi et al. derived the stability condition for the coupling motion on a sun-synchronous orbit based on a linearization of the motion [27]. On the control of the motion, Wang and Xu discussed the feedback orbit–attitude control for hovering using the noncanonical Hamiltonian structure [28]. In the framework of geometric mechanics, Lee et al. discussed a continuous finite-time control scheme used for body-fixed hovering over an asteroid [29]. Misra et al. further applied the scheme to soft landing on a tumbling asteroid [30]. Using visual odometry, Kulamani et al. investigated the geometric control for landing trajectories with a dumbbell spacecraft model [31]. Motivated by Lian et al.'s work [21], Viswanathan et al. analyzed the controllability of spacecraft with only attitude actuation and proved the drift vector field of an underactuated spacecraft near small bodies was weakly positively Poisson stable, which was a novel idea for spacecraft control near small bodies [32]. Furthermore, using gravitational orbit–attitude coupling, Wang and Xu found that body-fixed hovering at a given attitude could be achieved for a wide range of longitudes, with or without orbit control [26].

This work extends prior research by showing the feasibility of tracking a desired position trajectory to land on the surface of a small body or orbit the small body using only attitude control and gravitational orbit–attitude coupling. The main contributions of this paper are listed as follows:

- 1) The polyhedron model of an asteroid is applied to investigate the coupling motion.
- 2) A distributed point-mass model is developed to describe the attitude motion of the spacecraft.

3) Controllability of the underactuated spacecraft with only attitude control is verified with the polyhedron model of asteroid gravity.

4) A trajectory tracking scheme for the spacecraft in the vicinity of the asteroid using only attitude actuation is proposed based on the effect of gravitational orbit–attitude coupling.

This study can be considered as an application of gravitational orbit–attitude coupling to control trajectories in the vicinity of small bodies.

The polyhedral model has been proved to be a more accurate description of the gravitational field of an irregular-shaped small body than spherical harmonic expansions, especially near the surface of the small body [33]. The polyhedral model has been applied to study particle motions in the vicinity of an asteroid [6,8,11]. Here, we apply the polyhedron model to the coupled orbit and attitude motion of the spacecraft to increase accuracy. A distributed point-mass model (DPMM) that uses several mass points to obtain the total mass and moment of inertia of a spacecraft is built, which balances the accuracy of the attitude motion of the spacecraft and the computational efficiency during the full dynamics simulation. The simulation shows that the coupled motion using the polyhedron model shows distinct differences from the coupled motion in the spherical harmonic model. The polyhedron model with the distributed point-mass model can provide a more precise result for a coupling motion analysis.

Next, based on the research of Viswanathan et al. [32], the controllability of a spacecraft with only attitude actuation near irregularly shaped small solar system bodies is verified numerically, for which the Lie algebra rank condition for the polyhedron model is derived. This means the spacecraft can control its rotational and translational motions in the small-body proximity environment with only an attitude control system due to the effect of gravitational orbit–attitude coupling. A trajectory tracking scheme for the rigid body with only attitude control is proposed. The desired position trajectory that is tracked is generated by assuming a point-mass model, which is an initial assumption made in several small-body proximity missions [34,35]. The perturbation generated by the gravitational orbit–attitude coupling is considered as the control force to track the desired position trajectory. A nonlinear control method is applied to design the virtual control thrust, and the best attitude of the spacecraft is found for which the perturbation caused by the coupling is closest to the designed virtual control thrust. Finally, a finite-time stable attitude control is adopted to change the attitude of the spacecraft and achieve the virtual thrust. The results show that the proposed tracking scheme can keep the spacecraft close to the reference trajectory without requiring any orbit control. It increases the landing accuracy to 0.3 m and keeps the tracking error less than 7 m in 11 days, which reduces the requirement of orbit control, therefore saving on fuel consumption. It can also be regarded as a redundant control scheme that can be used in the event of thruster failures. This method can provide a reference for onboard control in future small-body missions.

The paper is organized as follows. Section II describes the coordinate frames and dynamics. The polyhedron model of an asteroid is introduced, and a distributed point-mass model is developed for the spacecraft. The discretized equations of motion are described. A trajectory tracking method based on gravitational orbit–attitude coupling is investigated in Sec. III. The calculation of controllability for the polyhedron model is derived. A nonlinear control method is used to design virtual control thrust, followed by the attitude optimization and a stable attitude control scheme. In Sec. IV, the full dynamics simulations are presented based on the polyhedron model and the DPMM. The feasibility of the proposed trajectory tracking scheme is verified. The conclusions are summarized in Sec. V.

## II. Dynamics Model for the Full-Body Problem

### A. Coordinate Frame Definition

The configuration space of spacecraft and asteroids is the special Euclidean group  $SE(3)$ , which is the set of all translational and rotational motions of a rigid body [36].  $SE(3)$  is a Lie group and can

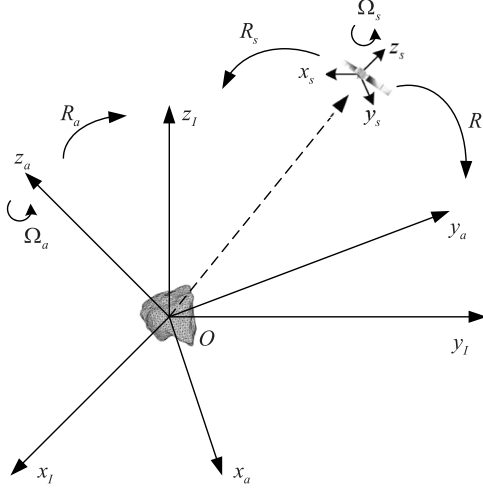


Fig. 1 Coordinate frames and position vectors.

be expressed as the semidirect product  $SE(3) \simeq \mathbb{R}^3 \times SO(3)$ , where  $\mathbb{R}^3$  is the three-dimensional real Euclidean space of positions of the mass center and  $SO(3)$  is the Lie group of orientations of the rigid body.

To analyze the motion in the vicinity of a small body, three coordinate frames are defined in this study: the asteroid-centered inertial frame  $\{\mathbb{I}\}^a$ , asteroid-fixed frame  $\{\mathbb{B}\}^a$ , and spacecraft body-fixed frame  $\{\mathbb{B}\}^s$ . The three axes of the asteroid-fixed frame are aligned with the principal axes of inertia of the asteroid, in which the  $X$  axis is the largest inertia axis and the  $Z$  axis is the smallest. The inertial frame coincides with the asteroid-fixed frame at the initial time and keeps the direction fixed in inertial space. The asteroid attitude is represented by the rotation matrix  $R_a \in SO(3)$  that transforms from the asteroid-fixed frame to the inertial frame. The spacecraft body-fixed frame has a similar definition. The three coordinate axes are along the principal axes of the spacecraft. Its attitude is denoted by  $R_s \in SO(3)$ , which transforms from the body-fixed frame to the inertial frame. Therefore, the rotation matrix  $R = R_a^T R_s \in SO(3)$  transforms from the body-fixed frame to the asteroid-fixed frame. The origin of the inertial frame coincides with the origin of the asteroid-fixed frame. The position and velocity vectors of the spacecraft in the inertial frame are defined by  $x \in \mathbb{R}^3$  and  $v = \dot{x} \in \mathbb{R}^3$ , respectively. The angular velocity vector of the asteroid is denoted by  $\Omega_a \in \mathbb{R}^3$  in  $\{\mathbb{B}\}^a$ , and the translational and angular velocity vectors of the spacecraft are denoted by  $\nu \in \mathbb{R}^3$  and  $\Omega_s \in \mathbb{R}^3$  in  $\{\mathbb{B}\}^s$ , respectively. The coordinate frames and position vectors are shown in Fig. 1.

## B. Asteroid Dynamics

In this paper, the asteroid is assumed to be a rigid body that moves around the sun with a known orbit. The relative motion between the asteroid and the spacecraft is considered, and it is described in the asteroid-centered inertial frame. This neglects the translational motion of the asteroid and considers only its attitude motion. The translational motion of the asteroid can be found in prior work [25]. The rotational kinematics of the asteroid can be expressed as

$$\dot{R}_a = R_a(\Omega_a)^\times \quad (1)$$

where  $(\cdot)^\times: \mathbb{R}^3 \rightarrow \mathfrak{so}(3)$  denotes the cross-product operator defined by

$$v^\times = \begin{bmatrix} 0 & -v_3 & v_2 \\ v_3 & 0 & -v_1 \\ -v_2 & v_1 & 0 \end{bmatrix} \quad (2)$$

Here,  $\mathfrak{so}(3)$  is the Lie algebra of  $SO(3)$ , which is represented as a  $3 \times 3$  skew-symmetric matrix.

Therefore, the attitude dynamics equation of the asteroid in the asteroid-fixed frame is given by

$$J_a \dot{\Omega}_a = J_a \Omega_a \times \Omega_a + M_a \quad (3)$$

where  $M_a \in \mathbb{R}^3$  is the gravity gradient moment acting on the asteroid (due to the sun and the spacecraft), and  $J_a$  is the moment of inertia of the asteroid, which are both expressed in  $\{\mathbb{B}\}^a$ . In this paper, we assume the asteroid is far larger than the spacecraft and neglect the moment due to the sun on the asteroid. Under this assumption,  $M_a = 0$ .

## C. Polyhedron Model of Asteroid

To reflect the irregular shape of the asteroid and get an accurate gravitational potential model, the homogeneous polyhedron model of an asteroid is used to describe its gravitational field [37]. This method does not face issues due to truncation errors (in series expansions) and keeps its convergence properties outside the shape model. Therefore, it can describe the gravity field of an asteroid more precisely than traditional spherical or elliptical harmonic expansions [33]. Polyhedron models have been used to investigate the precise particle dynamics around an asteroid [8,11]. Here, we extend it to study the coupled orbit-attitude motion of the rigid spacecraft.

The polyhedron model is defined by a series of vectors in the body-fixed frame, which define vertices that compose the surface of the asteroid. Three adjacent vertices  $i$ ,  $j$ , and  $k$  in a counterclockwise direction define a face and three edges. The potential of the polyhedron model at point  $P$  with position vector  $X$  in  $\{\mathbb{B}\}^a$  can be transferred to the integral of its faces and corresponding edges. The general formula can be expressed as

$$U(X) = \frac{1}{2} G \sigma \sum_{e \in \text{edges}} L_e r_e^T E_e r_e - \frac{1}{2} G \sigma \sum_{f \in \text{faces}} \omega_f r_f^T F_f r_f \quad (4)$$

where  $G$  is the gravity constant;  $\sigma$  is the density of the asteroid; and  $r_e$  and  $r_f$  are the vectors from a point on edge  $e$  and face  $f$  to point  $P$ , respectively.  $L_e$  represents the line factor, and  $\omega_f$  represents the face factor.  $E_e$  is the edge dyad, and  $F_f$  is the face dyad. The detailed expressions can be found in Ref. [37].

Besides, the gravity force, Hessian matrix, and Laplacian of the polyhedron are expressed as

$$\nabla U(X) = -G \sigma \sum_{e \in \text{edges}} L_e E_e r_e + G \sigma \sum_{f \in \text{faces}} \omega_f F_f r_f \quad (5)$$

$$\nabla \nabla U(X) = G \sigma \sum_{e \in \text{edges}} L_e E_e - G \sigma \sum_{f \in \text{faces}} \omega_f F_f \quad (6)$$

$$\nabla^2 U(X) = -G \sigma \sum_{e \in \text{edges}} \omega_f \quad (7)$$

The Laplacian can be used to determine whether the field point is outside or inside the polyhedron. The sum equals  $-4\pi$  when point  $P$  is inside, and it vanishes outside the polyhedron.

## D. Distributed Point-Mass Model and Spacecraft Dynamics

To demonstrate the effects of gravitational orbit-attitude coupling on a spacecraft, the shape and size of the spacecraft should be considered. One of the challenges for a rigid spacecraft model is the calculation of the gravity force and the moment from the polyhedron model of the asteroid. Fahnestock and Scheeres developed a method to obtain the mutual potential and the derivatives of potential between two polyhedron models and applied it to simulate the motion of binary asteroids [38]. But, the algorithm required heavy computations. The dumbbell shape has

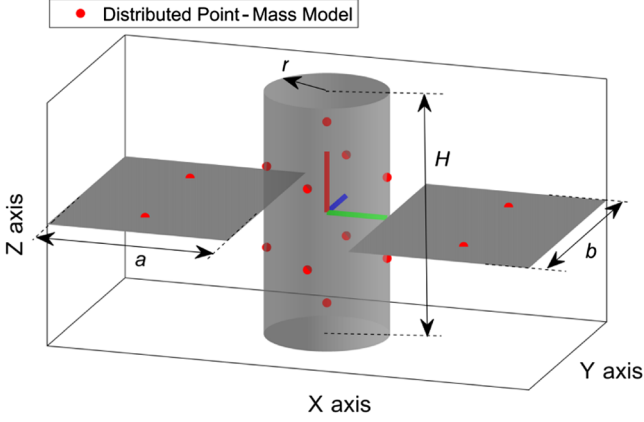


Fig. 2 Rigid spacecraft model and distributed point-mass model.

also been used to approximate a spacecraft [31,39]. But, those models do not reflect the inertia moment of spacecraft correctly, which impacted the accuracy of the attitude dynamics. In this paper, instead of a polyhedron model or a dumbbell-shaped model of the rigid spacecraft, a distributed point-mass model is developed, in which several mass points are used to obtain the total mass  $m$  and the moment of inertia  $J_s$  of the spacecraft. The relative position of each mass point is fixed in the body-fixed frame of the spacecraft. Here, we assume a common spacecraft design like Hayabusa, which contains two flat solar panels and one central body. The central body is considered to be a cylinder with its spin axis aligned with the body  $Z$  axis. Two solar panels are considered as rectangular plates in the  $XY$  plane passing through the  $X$  axis. The model of the rigid spacecraft in the body-fixed frame is shown in Fig. 2.

Ten points with different mass values are selected for the cylinder, for which two points of mass  $m_{c1}$  are set along the  $Z$  axis and the other eight points with mass  $m_{c2}$  are symmetrically located on the  $XZ$  plane and the  $YZ$  plane. Four equal mass points with mass  $m_{p1}$  are used to approximate the solar panels. The distributed point-mass model is marked in Fig. 2. It is assumed that the mass of the cylinder is  $m_c$  with height  $H$  and radius  $r$ , and the mass of each panel is  $m_p/2$  with length  $a$  and width  $b$ . The position and mass of each mass point in the body-fixed frame are listed in Table 1.

According to the polyhedron model, the force due to the gravitational potential field of an asteroid to the DPMM is the summation of the forces on each mass point. Denote the position of the center of the DPMM in  $\{\mathbb{B}\}^a$  as  $X = R_a^T x$  and the position vector of each mass point in  $\{\mathbb{B}\}^s$  as  $p_i (i = 1, 2, \dots, 14)$ . The total gravity force  $F \in \mathbb{R}^3$  on the DPMM in  $\{\mathbb{B}\}^a$  is

$$F(X, R) = \sum_{i=1}^{14} m_i \nabla U(X + R p_i) \quad (8)$$

where  $m_i$  is the mass for the  $i$ th mass point.

The gravity gradient moment  $M \in \mathbb{R}^3$  in  $\{\mathbb{B}\}^s$  can be expressed as

$$M(X, R) = \sum_{i=1}^{14} p_i \times R^T m_i \nabla U(X + R p_i) \quad (9)$$

Table 1 Parameters for distributed point-mass model

Mass points	Position	Mass
1–2	$[0, 0, \pm(\sqrt{5}/6)H]$	$m_{c1}^a$
3–6	$[\pm r, 0, \pm(H/6)]$	$m_{c2}^b$
7–10	$[0, \pm r, \pm(H/6)]$	$m_{c2}$
11–14	$[\pm\sqrt{(a^2/3) + r^2 + ar}, \pm(2\sqrt{3}/12)b, 0]$	$m_{p1}^c$

<sup>a</sup> $m_{c1} = m_c/4$ .

<sup>b</sup> $m_{c2} = m_c/16$ .

<sup>c</sup> $m_{p1} = m_p/4$ .

The kinematics for the spacecraft is given by the following:

$$\dot{g} = g(\xi)^\vee, \text{ where } (\xi)^\vee = \begin{bmatrix} \Omega_s^\times & \nu \\ 0 & 0 \end{bmatrix} \in \mathfrak{se}(3) \text{ and } g = \begin{bmatrix} R_s & x \\ 0 & 1 \end{bmatrix} \in \text{SE}(3) \quad (10)$$

Here,  $\mathfrak{se}(3)$  denotes the Lie algebra of the Lie group and  $\text{SE}(3)$  is the configuration, which is isomorphic to  $\mathbb{R}^6$  as a vector space.

The state space for the motion of the spacecraft is  $\text{TSE}(3) \approx \text{SE}(3) \times \mathfrak{se}(3)$ . The dynamics equations of motion for the spacecraft evolves on  $\text{TSE}(3)$  as follows:

$$m\dot{\nu} = m\nu \times \Omega_s + R^T F(X, R) + \phi_c \quad (11)$$

$$J_s \dot{\Omega}_s = J_s \Omega_s \times \Omega_s + M(X, R) + \tau_c \quad (12)$$

where  $\phi_c \in \mathbb{R}^3$  is the control force, and  $\tau_c \in \mathbb{R}^3$  is the control torque on the spacecraft, both in  $\{\mathbb{B}\}^s$ . The total mass of the DPMM is

$$m = \sum_{i=1}^{14} m_i$$

To summarize Eqs. (3) and (10–12), the full dynamics equation for the distributed point-mass model can be written as

$$\begin{cases} \dot{V} + \Omega_a \times V = \frac{F(X, R)}{m} + R \frac{\phi_c}{m} \\ J_s \dot{\Omega}_s = J_s \Omega_s \times \Omega_s + M(X, R) + \tau_c \\ J_a \dot{\Omega}_a = J_a \Omega_a \times \Omega_a \\ \dot{X} + \Omega_a \times X = V \\ \dot{R} = R(\Omega)^\times - (\Omega_a)^\times R \end{cases} \quad (13)$$

where  $V = R_a^T \dot{x} \in \mathbb{R}^3$  and  $\Omega = R\Omega_s \in \mathbb{R}^3$  are the translational velocity and the angular velocity of the spacecraft in  $\{\mathbb{B}\}^a$ .

## E. Discretization of Dynamics Models

Commonly used numerical integration methods, such as Runge–Kutta algorithms, suffer from issues of poor accuracy and maintaining state-space geometry while integrating continuous dynamics on Lie groups [40]. Therefore, the dynamics of the asteroid and the spacecraft are numerically integrated using a Lie group variational integrator (LGVI) in this paper. A variational integrator is derived by discretizing the variational principles of mechanics that lead to the equations of motion rather than discretizing the equations of motion directly. The Lie group variational integrator has desirable properties such as symplecticity, momentum preservation, and good energy stability for long time periods. It also requires a lower number of calculations per step, which makes it suitable for the polyhedron method.

Lee et al. derived the discrete equation of motion in both the inertial frame and the relative frame for two rigid bodies [40]. Like the continuous dynamics equation, the force and moment on the asteroid are neglected and only the force and moment on the spacecraft are considered.

Define the attitude variables  $F_k \in \text{SO}(3)$ ,  $F_{s_k} \in \text{SO}(3)$ , and  $F_{a_k} \in \text{SO}(3)$  as  $R_{a_{k+1}} = R_{a_k} F_{a_k}$ ,  $R_{s_{k+1}} = R_{s_k} F_{s_k}$ , and  $R_{k+1} = F_{a_k}^T F_k R_k$ , where  $F_{k+1} = R_k F_{s_k} R_k^T \cdot R_{a_k}$ ,  $R_{s_k}$ , and  $R_k$  represent the attitudes of the asteroid and the spacecraft, and the relative attitude of the spacecraft with respect to the asteroid, in discrete time. The discrete equations of relative motion are obtained as

$$\begin{cases}
X_{k+1} = F_{a_k}^T \left\{ X_k + h \frac{\Gamma_k}{m} - \frac{h^2}{2m} [F(X_k, R_k) - R_k \phi_{c_k}] \right\} \\
\Gamma_{k+1} = F_{a_k}^T \left\{ \Gamma_k - \frac{h}{2} [F(X_k, R_k) - R_k \phi_{c_k}] \right\} - \frac{h}{2} [F(X_{k+1}, R_{k+1}) - R_{k+1} \phi_{c_{k+1}}] \\
\Pi_{s_{k+1}} = F_{a_k}^T \left[ \Pi_{s_k} - \frac{h}{2} (M_k + \tau_{c_k}) \right] - \frac{h}{2} (M_{k+1} + \tau_{c_{k+1}}) \\
\Pi_{a_{k+1}} = F_{a_k}^T \Pi_{a_k} \\
R_{k+1} = F_{a_k}^T R_k \\
h \left[ \Pi_{s_k} - \frac{h}{2} (M_k + \tau_{c_k}) \right]^\times = F_{s_k} J_{d_s} - J_{d_s} F_{s_k}^T \\
h \Pi_{a_k}^\times = F_{a_k} J_{d_a} - J_{d_a} F_{a_k}^T
\end{cases} \quad (14)$$

where  $\Gamma_k = mV_k$  is the linear momentum of the spacecraft in  $\{\mathbb{B}\}^a$ ,  $\Pi_{s_k} = J_s \Omega_{s_k}$  is the angular momentum of the spacecraft in  $\{\mathbb{B}\}^s$ ,  $\Pi_{a_k} = J_a \Omega_{s_a}$  is the angular momentum of the asteroid in  $\{\mathbb{B}\}^a$ , and  $h$  is the integration step size.  $J_{d_s}$  and  $J_{d_a}$  are the nonstandard moments of inertia, which can be derived from

$$J_{d_a} = \frac{1}{2} \text{tr}[J_a] I_{3 \times 3} - J_a \quad (15)$$

$$J_{d_s} = \frac{1}{2} \text{tr}[J_s] I_{3 \times 3} - J_s \quad (16)$$

where  $J_a$  and  $J_s$  are the inertias of the asteroid and the spacecraft in their respective body-fixed frames.

The discrete time Hamiltonian map

$$\left( R_{s_k}, X_k, \Pi_{s_k}, \Gamma_k, R_{a_k}, \Pi_{a_k} \right) \rightarrow \left( R_{s_{k+1}}, X_{k+1}, \Pi_{s_{k+1}}, \Gamma_{k+1}, R_{a_{k+1}}, \Pi_{a_{k+1}} \right)$$

given by Eq. (14) provides a numerical integration scheme to numerically simulate the full dynamics of the DPMM.

### III. Trajectory Tracking Control Schemes Using Only Attitude Actuation

Consider the dynamics given in Eq. (13), for which the gravitational effect of  $F(X, R)$  is given by Eq. (6) and is dependent on the spacecraft attitude  $R_s$ . Due to the gravitational orbit–attitude coupling, the translational motion of rigid spacecraft in the proximity of a small solar system body can be controlled by attitude control torques alone. The authors of Ref. [32] studied the nonlinear controllability of the complete attitude and translational motion of a rigid spacecraft near a small solar system body using only attitude actuation. They used the results on weakly positively Poisson stable drift vector fields along with the Lie algebra rank condition (LARC) to conclude the controllability of the translational and rotational motions of the spacecraft under certain initial conditions. Here, we verify the controllability using the polyhedron model and propose a new orbit tracking method. Instead of separate translational control, it takes advantage of the gravitational orbit–attitude coupling and controls the attitude of the spacecraft to generate a virtual control force for trajectory tracking.

The overall scheme of the trajectory generation and tracking is as follows.

1) In step 1, a trajectory designed from a point-mass model without the effect of gravitational orbit coupling is taken as the reference trajectory. It provides a series of waypoints for tracking.

2) In step 2, the full dynamics is considered with the identical position and translational velocity. Due to the effect of the gravitational orbit–attitude coupling, the position trajectory under full dynamics deviates from the reference trajectory. The error between the reference and actual trajectories is calculated, and the

“virtual control thrust” that will track the reference trajectory is designed.

3) In step 3, an optimal attitude of the spacecraft is found, for which the perturbation caused by the gravitational orbit–attitude coupling is closest to the desired virtual control thrust by numerically solving it as an optimization problem.

4) In step 4, the spacecraft needs to track the desired attitude to provide the gravitational orbit–attitude coupling-generated control force required to track the reference trajectory. A finite-time attitude tracking controller is designed to track the calculated optimal attitude until the next optimal attitude state is generated.

Figure 3 shows the flowchart of the proposed scheme. In the following subsections, we explain each step in detail.

#### A. Virtual Control Thrust Design

The reference trajectory is designed, based on the motion of a spacecraft modeled as a point mass in the gravity of the asteroid represented using the polyhedron model. Let  $x_p$  and  $v_p$  denote the position and velocity, respectively, of the point mass represented in

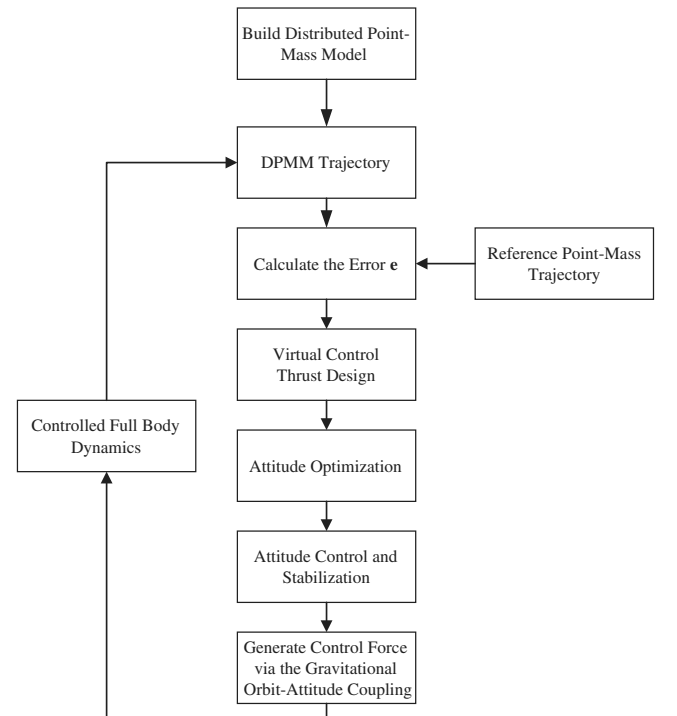


Fig. 3 Flowchart of the trajectory tracking scheme using the gravitational orbit–attitude coupling.

the inertial frame  $\{\mathbb{I}\}^a$ . The translational dynamics of the point-mass model is given by

$$\dot{x}_p = v_p \quad (17)$$

$$\dot{v}_p = \frac{1}{m} R_a \left( f_p(R_a^T x_p) \right) \quad (18)$$

where  $f_p(R_a^T x_p)$  is the thrust due to gravity on the point mass. From the polyhedron model, we have  $f_p(R_a^T x_p) = m \nabla U(X_p)$  in Eq. (5), where  $X_p$  equals  $R_a^T x_p$ . Note that the translational dynamics of the point mass is not dependent on the attitude of the spacecraft. Let  $x_d$  and  $v_d$  denote the position and velocity of the spacecraft with the DPMM in the coordinate frame  $\{\mathbb{I}\}^a$ . The translational dynamics of the DPMM can be rewritten to be

$$\dot{x}_d = v_d \quad (19)$$

$$\dot{v}_d = \frac{1}{m} R_a \left( F(R_a^T x_d, R) \right) + R_a u_{\text{virtual}} \quad (20)$$

where  $u_{\text{virtual}}$  is the virtual control thrust represented in frame  $\{\mathbb{B}\}^a$ . Let the position tracking error and velocity tracking error be defined as  $e_x = x_p - x_d$  and  $e_v = v_p - v_d$  respectively. The error dynamics can be expressed as

$$\dot{e}_x = e_v \quad (21)$$

$$\dot{e}_v = \frac{1}{m} R_a \left( F(X_p, R) - f_p(X_d) \right) + R_a u_{\text{virtual}} \quad (22)$$

Note that the error dynamics is complex and not necessarily an affine system in terms of the real control variable  $R_s$ . Additionally, an analytical expression of  $F(X, R)$  from the polyhedron model of the gravity would be too complicated. Instead, we design the virtual control  $u_{\text{virtual}}$  and reorient the spacecraft to achieve the virtual control thrust through gravitational orbit–attitude coupling:

$$u_{\text{virtual}} = R_a^T \left[ -K_x \tanh(K_x e_x) - \alpha_v \tanh(\beta_v e_v) \right] - \frac{1}{m} \left( F(X_p, R) - f_p(X_d) \right) \quad (23)$$

where  $K_x$  is the positive definite control matrix, and  $\alpha_v$  and  $\beta_v$  are positive control gains. Their values can be chosen by the magnitude of coupling. Function  $\tanh(\cdot)$  is operated componentwise on the vector. The stability property of the control law is shown in the following theorem.

*Theorem III.1:* Consider the error dynamics of Eqs. (21) and (22). Under the feedback control law for  $u_{\text{virtual}}$  given in Eq. (23), the feedback translational tracking error dynamics given by Eqs. (21) and (22) is stabilized to  $(e_x, e_v) = (0, 0)$  asymptotically.

*Proof:* The stability can be proved using the following Lyapunov function:

$$\mathcal{V}_{\text{tran}} = \log_e(\cosh(K_x e_x)) + \frac{1}{2} e_v^T e_v = \mathcal{V}(e_x, e_v) \quad (24)$$

where the  $\log_e(\cdot)$  and  $\cosh(\cdot)$  are operated componentwise. Take the derivate of  $\mathcal{V}_{\text{tran}}$  with respect to  $t$  to get

$$\begin{aligned} \frac{d}{dt} \mathcal{V}(e_x, e_v) &= (K_x \dot{e}_x)^T \tanh K_x e_x + \dot{e}_v^T e_v \\ &= e_v^T \left[ K_x \tanh K_x e_x - K_x \tanh K_x e_x - \alpha_v \tanh(\beta_v e_v) \right] \\ &= e_v^T \left[ -\alpha_v \tanh(\beta_v e_v) \right] \end{aligned} \quad (25)$$

Then, it has

$$\dot{\mathcal{V}}_{\text{tran}} = -\alpha_v e_v^T \tanh(\beta_v e_v) \leq 0$$

if  $\alpha_v > 0$  and  $\beta_v > 0$ . Thereafter, theorem 8.4 from Ref. [41] can be invoked to conclude that  $e_v \rightarrow 0$ , and thereafter  $e_x \rightarrow 0$  as  $t \rightarrow \infty$ .

As explained earlier, we assume no thrust control for the spacecraft, and the virtual control designed in Eq. (23) cannot be applied directly. The control effort  $u_{\text{virtual}}$  will be achieved using the gravitational orbit–attitude coupling in the following part.

## B. Controllability Analysis and Attitude Optimization

The virtual control given by Eq. (23) should be generated by changing the attitude of the spacecraft using gravitational orbit–attitude coupling. The spacecraft is an underactuated system if it is only controlled by attitude controllers. The system is shown to be controllable if its drift vector field is weakly positively Poisson stable and the system satisfies the Lie algebra rank condition [21].

The controllability of the spacecraft in the gravitational field of polyhedron model is derived at first. Assume that the attitude actuation can control all three rotational degrees of freedom  $b_i, i = 1, 2, 3$ . The spacecraft dynamics with only attitude actuation in the control affine form can be presented as follows:

$$\dot{\varphi} = f_c(\varphi) + \sum_{i=1}^3 u_i g_{c_i}(\varphi) \quad (26)$$

$$f_c = \begin{pmatrix} R_s (J_s^{-1} \Pi_s)^\times \\ R_s (J_s^{-1} \Pi_s)^\times \Pi_s^\times \\ \frac{R_a \Gamma}{m} \\ R_a F(X, R) \end{pmatrix}, \quad g_{c_i} = \begin{pmatrix} 0 \\ R_s b_i^\times \\ 0 \\ 0 \end{pmatrix}, \quad i = 1, 2, 3 \quad (27)$$

The configuration manifold is  $\mathbb{Q} = \text{SE}(3)$ , and a point on the cotangent bundle  $\varphi \in \mathbb{T}^* \mathbb{Q}$  is represented as  $\varphi = (R_s, R_s \Pi_s^\times, x, R_a \Gamma)$ . Let vector fields  $Y$  and  $Z$  at  $\varphi$  be written as

$$\begin{aligned} Y(\varphi) &= \left( R_s \zeta^\times, R_s (\zeta^\times \Pi_s^\times + \eta^\times), \lambda \right), \\ Z(\varphi) &= \left( R_s a^\times, R_s (a^\times \Pi_s^\times + d^\times), c \right) \end{aligned} \quad (28)$$

where  $\zeta, \eta, \lambda$ , and  $c$  are all functions of the states  $\varphi$ . The flows of  $Y$  and  $Z$  can be found to be

$$\psi_t^Y(\varphi) = \left( R_s e^{t \zeta^\times}, R_s e^{t \zeta^\times} (\Pi_s^\times + t \eta^\times), x + t \lambda \right) \quad (29)$$

$$\psi_t^Z(\varphi) = \left( R_s e^{t a^\times}, R_s e^{t a^\times} (\Pi_s^\times + t d^\times), x + t c \right) \quad (30)$$

The Lie bracket  $[Y, Z]$  can be computed as

$$[Y, Z](\varphi) = \frac{d}{dt} \Big|_0 \left( Z \circ \psi_t^Y(\varphi) - Y \circ \psi_t^Z(\varphi) \right) \quad (31)$$

Viswanathan et al. [32] proved that the drift vector field of an underactuated spacecraft near small bodies is weakly positively Poisson stable. Here, the controllability based on the polyhedron asteroid model and the DPMM for the spacecraft are derived. Let  $Y = f_c$  and  $Z = g_c$  with the associated terms

$$\begin{aligned} \zeta &= J_s^{-1} \Pi_s, \quad \eta = 0, \quad \lambda = \begin{pmatrix} \frac{R_a \Gamma}{m} \\ R_a F(X, R) \end{pmatrix}, \\ a &= 0, \quad d = b_i, \quad c = \begin{pmatrix} 0 \\ 0 \end{pmatrix} \end{aligned}$$

The Lie brackets for the underactuated system are computed as follows:

$$f_{c_i} \triangleq [f_c, g_{c_i}] = \begin{pmatrix} -R_s(J_s^{-1}b_i)^\times \\ -R_s(J_s^{-1}b_i)^\times \Pi_s^\times \\ 0 \\ 0 \end{pmatrix}, \quad i = 1, 2, 3$$

and

$$F_i \triangleq [f_c, f_{c_i}] = \begin{pmatrix} -R_s(J_s^{-1}\Pi_s \times J_s^{-1}b_i)^\times \\ -R_s(J_s^{-1}\Pi_s \times J_s^{-1}b_i)^\times \Pi_s^\times \\ 0 \\ F_{i,4} \end{pmatrix}, \quad i = 1, 2, 3$$

According to the previous result, the LARC is satisfied if the three vectors  $F_{i,4}$ ,  $i = 1, 2, 3$  are nonzero, where

$$F_{i,4} = \frac{d}{dt} \Big|_0 c \circ \psi_t^{f_c} - \frac{d}{dt} \Big|_0 \lambda \circ \psi_t^{f_{c_i}} = -\frac{d}{dt} \Big|_0 \lambda \circ \psi_t^{f_{c_i}}$$

and

$$\lambda = G\rho R_a \sum_{w=1}^{14} \left( -\sum_{e \in \text{edges}} L_e E_e r_e + \sum_{f \in \text{faces}} \omega_f F_f r_f \right) m(w)$$

According to the Lie bracket formula,  $F_{i,4}$  is evaluated as

$$\begin{aligned} F_{i,4} &= G\rho R_a \sum_{w=1}^{14} \left( \sum_{e \in \text{edges}} L_e E_e R e q_w^\times + \sum_{f \in \text{faces}} \omega_f F_f R f q_w^\times \right) m(w) J_s^{-1} b_i \\ &+ G\rho R_a \sum_{w=1}^{14} \left( \sum_{e \in \text{edges}} \frac{\partial L_e}{\partial t} \Big|_{t=0} E_e r_e + \sum_{f \in \text{faces}} \frac{\partial \omega_f}{\partial t} \Big|_{t=0} F_f r_f \right) m(w) \end{aligned} \quad (32)$$

The numerical simulation in Sec. IV shows that the three vectors  $F_{1,4}$ ,  $F_{2,4}$ , and  $F_{3,4}$  are nonzero and linearly independent in the vicinity of the asteroid. In that case, with the drift vector field being weakly positively Poisson stable, the spacecraft is controllable using only attitude control in the vicinity of the irregular asteroid, which means the spacecraft can change its attitude to generate the control force using gravitational orbit–attitude coupling.

Note the initial state of spacecraft as  $X_0, \Phi_0$ . Here, the attitudes of the spacecraft are given by exponential coordinates

$$\Phi = [\Phi_1, \Phi_2, \Phi_3]^T, \quad \Phi_i \in (-\pi, \pi], \quad i = 1, 2, 3$$

to avoid the singularity. The transformation between  $\Phi$  and the rotation matrix  $R_s$  is shown as

$$R_s = \exp(\Phi^\times) = I_{3 \times 3} + \frac{\sin \|\Phi\|}{\|\Phi\|} \Phi^\times + \frac{1 - \cos \|\Phi\|}{\|\Phi\|^2} (\Phi^\times)^2 \quad (33)$$

The gravitational force to the DPMM is

$$F_0 = F(R_a(t), R_s(\Phi_0), X_0)$$

The optimal attitude and the corresponding gravitational force are noted as  $\Phi^*$  and

$$F_1^* = F(R_a(t), R_s(\Phi^*), X_0)$$

which should satisfy the equation

$$F_1^* - F_0 = u_{\text{virtual}}$$

As the magnitude of the coupling effect is limited and varies with position, the control acceleration may not be satisfied completely.

In that case, the attitude that minimizes the error between the actual control acceleration  $\hat{u} = F_1 - F_0$  and the desired control acceleration  $u_{\text{virtual}}$  is determined as the optimal attitude  $\Phi^*$ . The cost index of the optimal problem is described as

$$\min_{\hat{u}} J(\Phi) = \|\hat{u} - u_{\text{virtual}}\| \quad (34)$$

By algebraic optimization methods such as conjugate gradient algorithms, the optimal attitude can be found. The next part describes the attitude control scheme.

### C. Finite-Time Stable Attitude Tracking Control

The attitude control and stabilization enact the virtual thrust by reorienting the attitude of the spacecraft from the initial attitude  $\Phi_0$  to the optimal attitude  $\Phi^*$ . There are several control methods. Here, a finite-time state feedback tracking control scheme is applied [42,43]. Denote the desired attitude as  $R_d(\Phi^*)$  and the desired angular velocity as  $\Omega_d$ . The attitude tracking error is  $Q = R_d^T R_s$ . The kinematics for the tracking error is

$$\dot{Q} = Q(\omega)^\times \quad (35)$$

where  $\omega = \Omega_s - Q^T \Omega_d$  is the error in angular velocity in  $\{\mathbb{B}\}^s$ . The dynamics for the tracking errors in the angular velocity is

$$\begin{aligned} J_s \dot{\omega} &= \tau_c + J_s (\omega^\times Q^T \Omega_d - Q^T \dot{\Omega}_d) \\ &- (\omega + Q^T \Omega_d)^\times J_s (\omega + Q^T \Omega_d) + M(X, R) \end{aligned} \quad (36)$$

The following two lemmas are used to derive the feedback control torque  $\tau_c$ .

*Lemma III.1:* Let  $\alpha$  and  $\beta$  be nonnegative real numbers, and let  $p \in (1, 2)$ . Then,

$$\alpha^{(1/p)} + \beta^{(1/p)} \geq (\alpha + \beta)^{(1/p)} \quad (37)$$

This inequality is strict if both  $a$  and  $b$  are nonzero.

*Lemma III.2:* Let  $\langle K, I - Q \rangle = \text{trace}(K - KQ)$  denote a function that maps  $\text{SO}(3)$  to  $\mathbb{R}$ , where  $K = \text{diag}(k_1, k_2, k_3) \in \mathbb{R}^3$  is a diagonal gain matrix with  $k_1 > k_2 > k_3 \geq 1$ . Define

$$s_K(Q) = \sum_{i=1}^3 k_i (e_i)^\times (Q^T e_i) \quad (38)$$

such that

$$\frac{d}{dt} \langle K, I - Q \rangle = \omega^T s_K(Q)$$

which makes  $\langle K, I - Q \rangle$  a Morse function defined on  $\text{SO}(3)$ . Here,  $e_1 = [1 \ 0 \ 0]^T$ ,  $e_2 = [0 \ 1 \ 0]^T$ , and  $e_3 = [0 \ 0 \ 1]^T$  are the standard basis vectors.

Let  $\mathcal{S} \subset \text{SO}(3)$  be a closed subset containing the identity in its interior, defined as

$$\mathcal{S} = \{Q \in \text{SO}(3) : Q_{ii} \geq 0 \text{ and } Q_{ij} Q_{ji} \leq 0, \forall i, j \in \{1, 2, 3\}, i \neq j\}$$

Then, for  $Q \in \mathcal{S}$ , one obtains

$$s_K(Q)^T s_K(Q) \geq \langle K, I - Q \rangle \quad (39)$$

The finite-time attitude tracking control scheme is given as follows:

*Theorem III.2:*  $s_K(Q)$  Consider the attitude dynamics of Eq. (36) with in Eq. (38). Define

$$z_K(Q) = \frac{s_K(Q)}{(s_K^T(Q) s_K(Q))^{1-1/p}} \quad (40)$$

and

$$w(Q, \omega) = \frac{d}{dt} s_K(Q) = \sum_{i=1}^3 k_i e_i \times (\omega \times Q^T e_i) \quad (41)$$

where  $p \in (1, 2)$ . Furthermore, let  $L$  be a positive definite control gain matrix such that  $L - J_s$  is positive semidefinite, let  $k_p > 1$ , and define  $\kappa$  such that

$$\kappa^p = \frac{\sigma_{L, \min}}{\sigma_{J_s, \max}} > 0$$

The feedback control law for  $\tau_c$  is given by

$$\begin{aligned} \tau_c = & J_s \left( Q^T \dot{\Omega}_d - \frac{\kappa H(s_K(Q))}{(s_K^T(Q) s_K(Q))^{1-1/p}} w(Q, \omega) \right) \\ & + (Q^T \Omega_d) \times J_s \left( Q^T \Omega_d - \kappa z_K(Q) \right) + \kappa J_s \left( z_K(Q) \times Q^T \Omega_d \right) \\ & + \kappa J_s (\omega + Q^T \Omega_d) \times z_K(Q) - k_p s_K(Q) \\ & - \frac{L \Psi(Q, \omega)}{(\Psi(Q, \omega)^T L \Psi(Q, \omega))^{1-1/p}} - M(X, R) \end{aligned} \quad (42)$$

where

$$\Psi(Q, \omega) = \omega + \kappa z_K(Q) \quad (43)$$

and

$$H(x) = I - \frac{2(1-1/p)}{x^T x} x x^T \quad (44)$$

Then, the feedback attitude tracking error dynamics given by Eq. (36) is stabilized to  $(Q, \omega) = (I, 0)$  in finite time. The proof of the finite-time attitude tracking control scheme and its stability were given by Bohn and Sanyal [42], and it is omitted here for brevity.

At each instant, the error between the DPMM trajectory and the reference trajectory at the waypoint is calculated and the virtual control thrust is generated. The finite-time stable attitude tracking control will drive the attitude of the spacecraft to the optimal reference attitude in a stable manner until the spacecraft reaches the next waypoint and updates the desired attitude. The time interval between successive waypoints is denoted as  $h_c$ , which is greater than the integration step size  $h$ .

#### IV. Numerical Validation

In this section, the full dynamics simulation of the spacecraft close to an asteroid is shown. Asteroid 101955 Benu, which is the target for the ongoing Origins Spectral Interpretation Resource Identification Security Regolith Explorer (OSIRIS-REx) mission, is considered in this simulation. For a small-body proximity mission, the spacecraft trajectory in proximity to the body is usually designed based on the point-mass (PM) model, as can be found in various studies and actual mission designs [34,35]. Given this background for prior and current missions, we choose a point-mass trajectory as the reference trajectory. First, simulations showing the gravitational coupling are presented based on the polyhedron model and the distributed point-mass model, and then the results are compared with the point-mass model. The corresponding motions in the spherical harmonic gravitational field of the asteroid are also developed as a contrast. Two cases are discussed around the asteroid: the ballistic landing trajectory from an analogous equilibrium point of the asteroid, and the elliptic orbit around the asteroid. Second, the proposed tracking method using only attitude actuation is shown in the two cases to verify its feasibility.

##### A. Effect of Gravitational Orbit–Attitude Coupling

The polyhedron gravity model and spherical harmonic expansion gravity model of Benu are used in this simulation. The polyhedron

**Table 2** Parameters for asteroid 101955 Benu [44,46]

Parameter	Value
Density	$1.260 \times 10^3 \text{ kg/m}^3$
Size	$565 \times 535 \times 508 \text{ m}$
Volume	$0.0623 \text{ km}^3$
Moment of inertia	$\text{diag}[1.8235, 1.8946, 2.0453] \times 10^9 \text{ kg}^* \text{m}^2$
Rotation period	4.297 h

**Table 3** Parameters for spacecraft

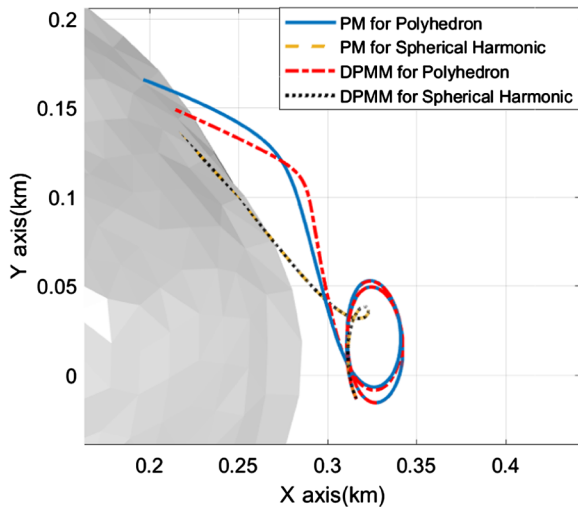
Parameter	Value
Total mass	500 kg
Mass of central part	400 kg
Mass of solar panels	100 kg
Moment of inertia	$\text{diag}[0.333, 0.583, 0.318] \times 10^3 \text{ kg}^* \text{m}^2$
Height of cylinder	3 m
Radius of cylinder	0.5 m
Length of solar panel	2 m
Width of solar panel	1 m

model is obtained based on observations in 1999 and 2005 [44]. Table 2 shows the parameters for Benu. The spherical harmonic expansion up to  $8 \times 8$  is obtained based on the polyhedron model [44–46]. The assumed parameters of the spacecraft are given in Table 3. Here, we focus on the motion close to the surface, where the irregular gravitational field of the asteroid dominates the motion. Therefore, we do not take the solar radiation pressure and third-body perturbation into consideration, and the control force and torque are set as  $\phi_c = 0$  and  $\tau_c = 0$ .

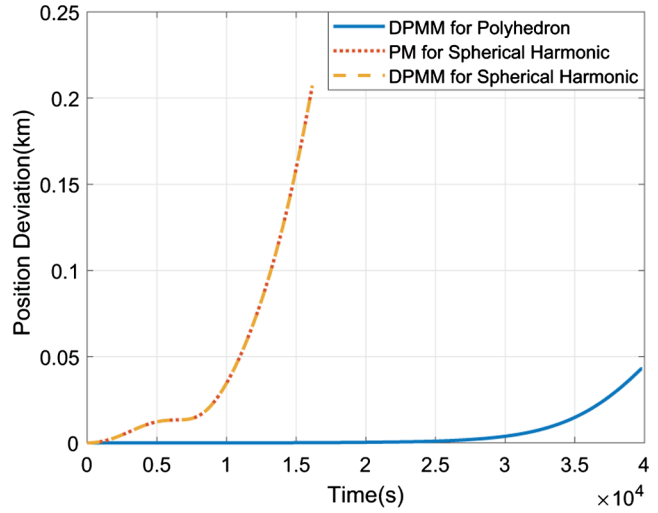
##### 1. Case 1: Landing Trajectory

The landing trajectory starts from the quasi-periodic orbit around the dynamic equilibrium point of the asteroid. Due to the irregular shape of the asteroid, the asteroid has an analogous equilibrium point, as in the circular restricted three-body problem (CRTBP) [8]. There are also similar periodic orbits around the equilibrium point, as well as associated invariant manifolds. The spacecraft on the periodic orbit can transfer along the unstable manifolds with a small perturbation and gradually land on the surface of the asteroid in several hours [47]. Here, the periodic orbit around the equilibrium point close to  $X$  axis is chosen. The designed landing site is a latitude of  $0.586^\circ$  and a longitude of  $40.090^\circ$  (the definition of positive longitude starts from the  $X$  axis counterclockwise).

The numerical simulation is carried out with an integration step size of  $h = 0.5 \text{ s}$ . The Laplacian in Eq. (7) is used to determine the landing state for polyhedron model. The initial relative position and velocity are  $[316.370 \ -13.602 \ -1.105] \text{ m}$  and  $[1.168 \ 137.965 \ 6.036] \times 10^{-3} \text{ m/s}$  in  $\{\mathbb{B}\}^a$ . The initial attitude of the spacecraft is  $[0, 0, 1]$  in exponential coordinates with zero angular velocity. Figure 4 shows the trajectories using different gravity models. As shown in Fig. 4a, due to the gravitational orbit–attitude coupling, the trajectory of the DPMM gradually shifts from the PM trajectory and lands on a different site. Taking the PM trajectory in the polyhedron model as a reference, the position deviations of the other three models with time are shown in Fig. 4b. It is found that both the DPMM trajectory and the PM trajectory using the spherical harmonic model are different from those obtained using the polyhedron model. As stated in previous literature [37], the spherical harmonic model is not guaranteed to converge inside the Brillouin sphere, which causes large gravity errors near the surface of the asteroid. The inaccuracy of the gravitational field leads to a 6 h difference in landing time for both the DPMM trajectory and the PM trajectory. The final position difference of the DPMM trajectory is also up to 33.1 m between the spherical harmonic model and the polyhedron model.



a) Landing trajectories for different models in the asteroid-fixed frame



b) Position deviations relative to point-mass trajectory in polyhedron model

Fig. 4 Comparison between different models for landing trajectory.

Table 4 Initial rotational states of the spacecraft for landing

State	Attitude $\Phi$ , rad	Angular velocity $\Omega_s$ , rad/s
$T_1$	[0 0 -1]	[0 0 0]
$T_2$	[0 0 0]	[0 0 0]
$T_3$	[-0.839 0.225 -1.482]	[0 0 0]
$T_4$	[-1.597 -0.542 -1.112]	[0 0 0]
$T_5$	[1.114 -0.299 -1.413]	[0 0 0]
$T_6$	[-1.209 -1.209 -1.209]	[1 0.2 0.1] $\times 10^{-3}$
$T_7$	[-0.541 -0.184 -1.404]	[1 0.2 0.1] $\times 10^{-3}$
$T_8$	[-0.598 0.079 -1.785]	[1 0.2 0.1] $\times 10^{-3}$
$T_9$	[-1.749 -0.230 -1.399]	[1 0.2 0.1] $\times 10^{-3}$
$T_{10}$	[-1.207 -0.500 2.091]	[1 0.2 0.1] $\times 10^{-3}$

Furthermore, we change the initial rotational states for the DPMM in the simulation, as listed in Table 4. A total of 10 different initial attitudes and angular velocities are chosen, namely,  $T_1$ – $T_{10}$ . The angular velocities are expressed in the body-fixed frame, and the attitudes of the spacecraft are given by exponential coordinates. Figure 5 illustrates landing trajectories starting from the same initial position and translational velocity but different initial attitudes and

angular velocities. As can be seen, due to the gravitational orbit–attitude coupling, the trajectories of the DPMM shift from the point-mass trajectory. By choosing different initial attitudes, the spacecraft with the same translational state will land on different areas of the asteroid. Some of the initial states may fly far away from the desired landing site, as shown in Fig. 5b. Figure 6 shows the distribution of actual landing sites by longitude and latitude for these different initial notational motion states. The maximum landing error is up to  $20^\circ$  in longitude and  $1^\circ$  in latitude, which is about 100 m in distance. The spacecraft will miss the intended landing site and make contact with the asteroid surface at different sites, which may adversely affect its scientific mission objectives. The coupling also changes the attitude of the spacecraft from its initial state, which may also cause an undesired landing attitude, resulting in possible damage to the spacecraft.

## 2. Case 2: Elliptic Orbit

In the second case, the initial trajectory starts from an elliptic orbit with an eccentricity of  $e = 0.15$  and a semimajor axis of  $a = 0.36$  km. The initial conditions are shown in Table 5. The trajectories are integrated for 11 days with an integration step size of  $h = 1$  s.

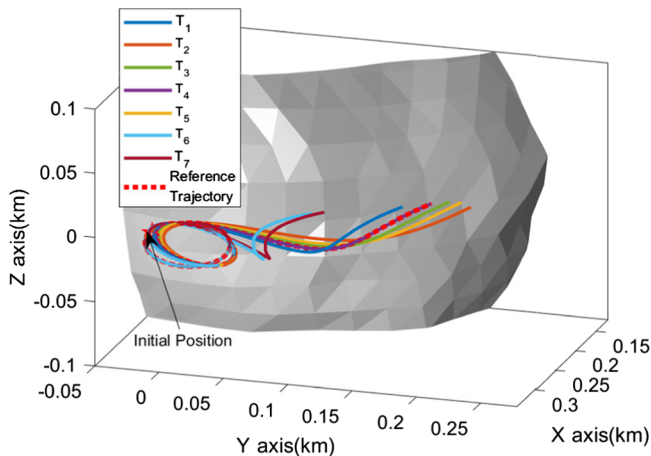
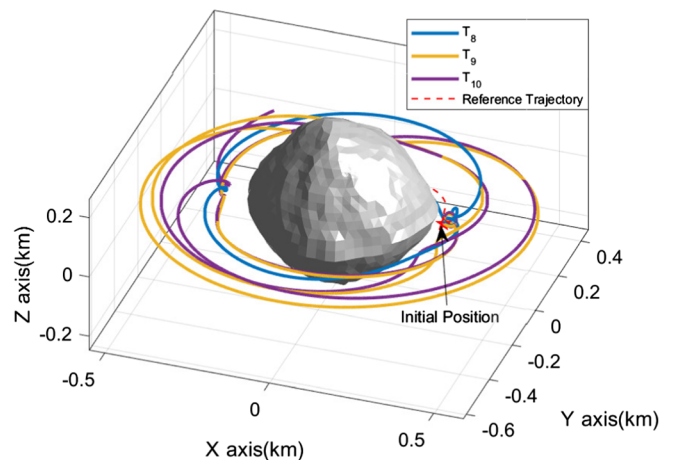

 a) Landing trajectories for state  $T_1$ – $T_7$ 

 b) Landing trajectories for state  $T_8$ – $T_{10}$ 

Fig. 5 Landing trajectories of the DPMM for different initial conditions.

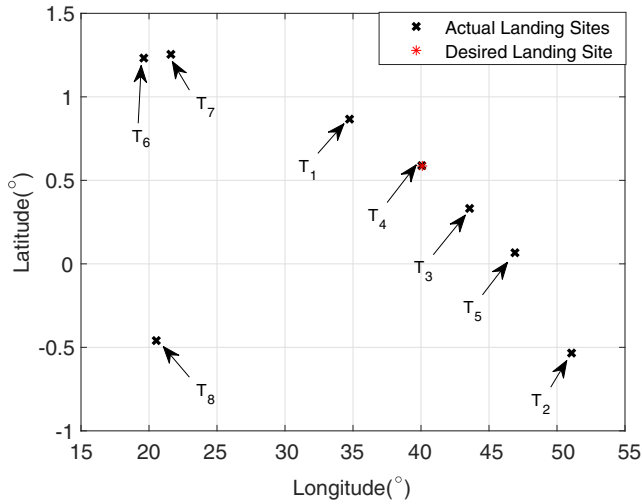
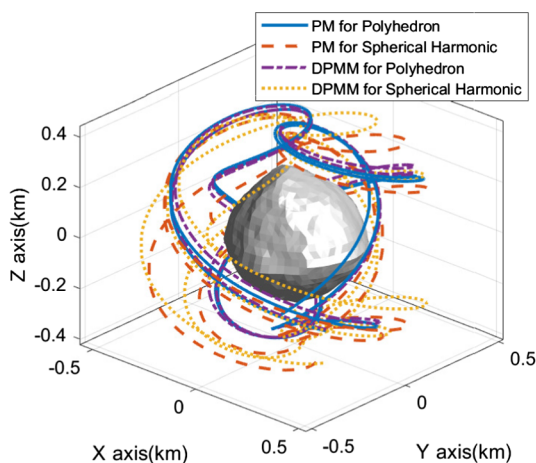


Fig. 6 Distribution of the landing sites for the DPMM and the point-mass model.

Table 5 Initial translational and rotational states of the spacecraft for the elliptic orbit

Initial states	Value
Relative position $X$ , m	[108.207 -284.253 -173.180]
Relative velocity $V$ , m/s	[6.014 -65.264 110.881] $\times 10^{-3}$
Attitude $\Phi$ , rad	[0 0 0]
Angular velocity $\Omega_s$ , rad/s	[0.1 0 0.2] $\times 10^{-3}$

Figure 7a shows the orbits in different models at the last day in the asteroid-fixed frame, and Fig. 7b shows the relative position errors for different models with PM orbits in the polyhedron model. Similar to landing trajectories, the gravitational orbit-attitude coupling causes the deviation of the DPMM orbit from the PM orbit. The position error induced by the coupling gradually increases with time. The maximum error is more than 100 m in the polyhedron model. The error also exists in the spherical harmonic model. Besides, the error between the DPMM orbit in the polyhedron model and that in the spherical harmonic model is up to 0.9 km, which reflects the effect of



a) Orbits for different models in the asteroid-fixed frame

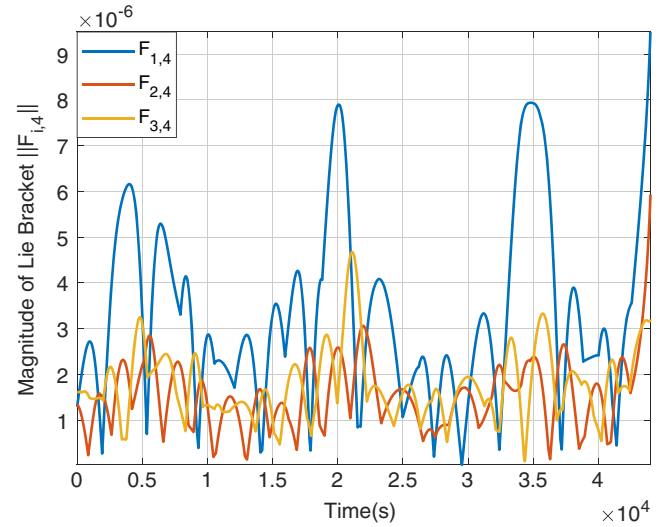


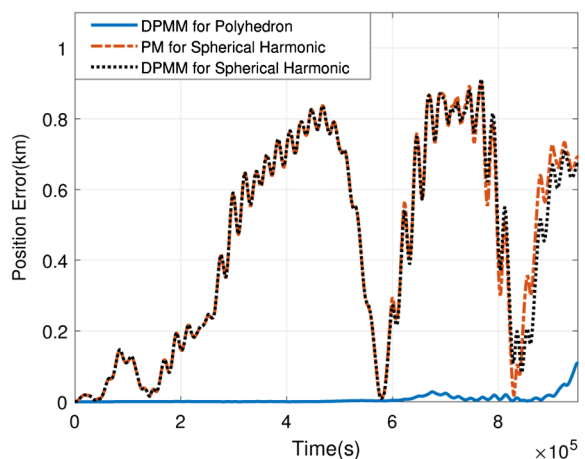
Fig. 8 Lie bracket  $F_{i,4}$  along the landing trajectory  $T_2$ .

the accuracy of the gravitational field model on the coupled orbit and attitude motion of the spacecraft.

## B. Tracking with Attitude Actuation

The aforementioned simulations of the natural full dynamics show that the gravitational orbit-attitude coupling causes the actual trajectory of a rigid-body spacecraft to deviate from the desired point-mass trajectory, and therefore orbit control is necessary. Instead of implementing the orbit correction by propulsive thrust force, the proposed trajectory tracking method uses only attitude control for trajectory tracking.

The numerical results of the controllability analysis using the polyhedron model are shown in Fig. 8. The magnitudes of vectors  $F_{1,4}$ ,  $F_{2,4}$ , and  $F_{3,4}$  along the landing trajectory  $T_2$  are nonzero and linearly independent for the polyhedron model of the asteroid and the DPMM of the spacecraft. The Lie brackets  $F_{i,4}$  along other trajectories show similar behaviors. In this case, the spacecraft is controllable using only attitude control in the vicinity of the irregular asteroid. Besides, it is found that larger  $F_{i,4}$  appear when the trajectory is close to the surface, which means the controllability increases with smaller orbit sizes. Moreover, the Lie brackets along



b) Position errors relative to point-mass trajectory in Polyhedron model

Fig. 7 Comparison between different models for elliptic orbits.

the trajectory for a uniform spherical asteroid are much smaller than in the polyhedron model (on the order of  $10^{-4}$  in magnitude). The irregular shape of the asteroid significantly increases the effect of gravitational orbit–attitude coupling.

The tracking scheme is applied to track the landing trajectory in case 1 and the elliptic orbit in case 2, respectively. The same spacecraft parameters and initial states of translational motion are used. The maximum perturbation due to the gravitational orbit–attitude coupling around Bennu is calculated about  $1.7 \times 10^{-6}$  N. Therefore, the gain values for trajectory tracking are selected as

$$K_x = 1.4 \times 10^{-3}, \quad \alpha_v = 1 \times 10^{-6}, \quad \beta_v = 1$$

For the landing trajectory, the initial attitude is selected to be identical to  $T_2$  in Table 4. The time interval between waypoints  $h_c$  is chosen as 100 s. Figure 9 shows the results in the asteroid-fixed frame. In contrast, the natural DPMM trajectory is also plotted. The position errors and attitudes of the spacecraft are shown in Figs. 10 and 11, respectively. The landing trajectory using the control scheme in Sec. IV increases the landing accuracy to less than 0.3 m, which is much better than the natural motion. Figure 12 shows the controlled

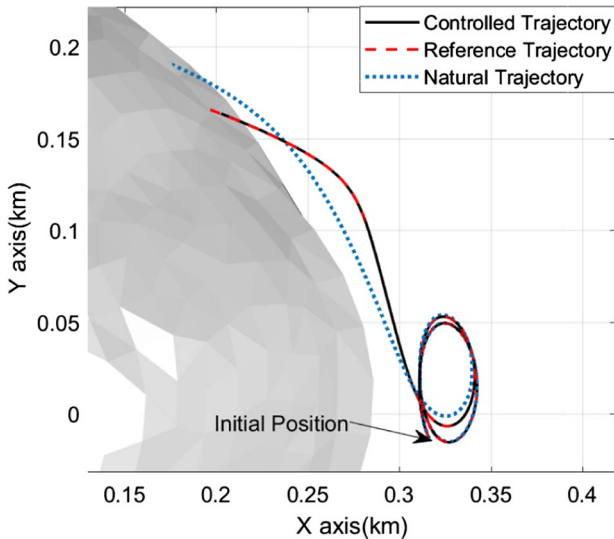


Fig. 9 Tracking landing trajectory in the asteroid-fixed frame.

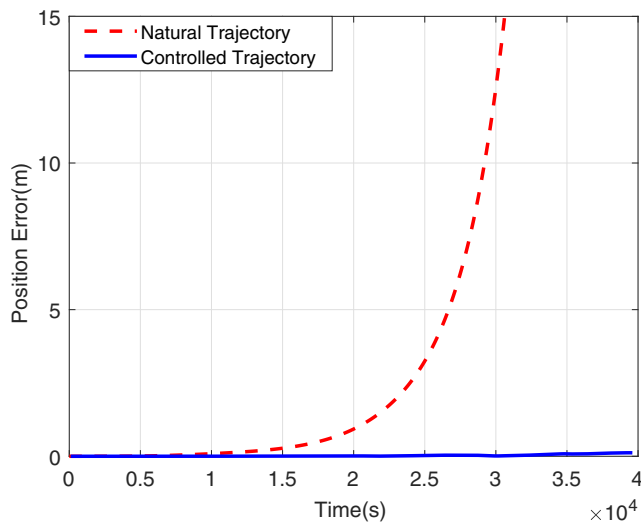


Fig. 10 Position error for the controlled landing trajectory.

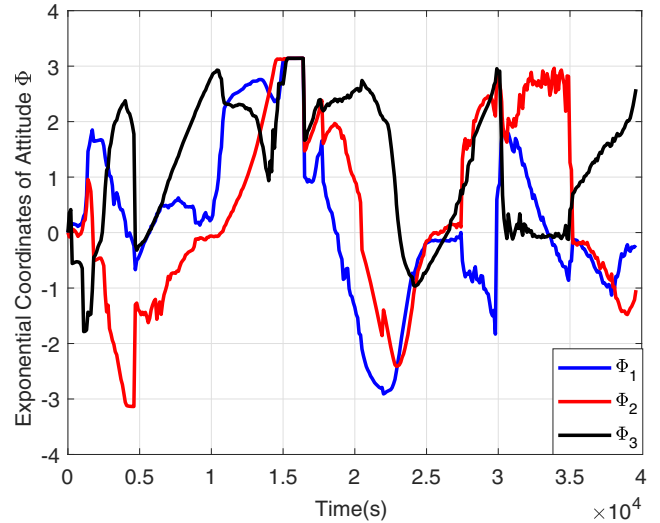


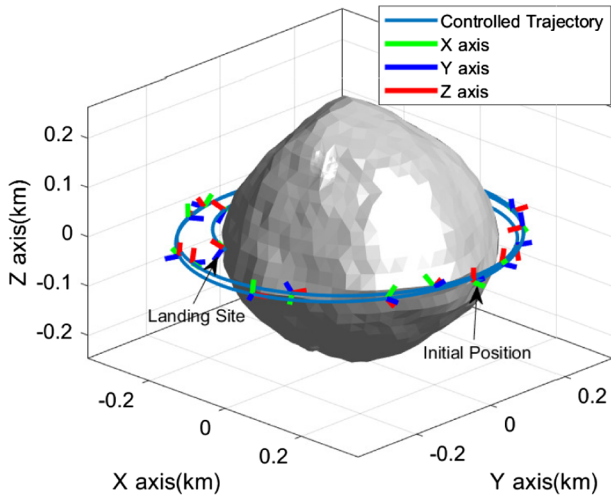
Fig. 11 Attitude of the spacecraft along the controlled landing trajectory.

landing trajectory in the inertial frame and the attitude of the spacecraft along the trajectory at a few waypoints. As shown in Figs. 11 and 12, the attitude of the spacecraft changes over time to match the desired control force and its direction.

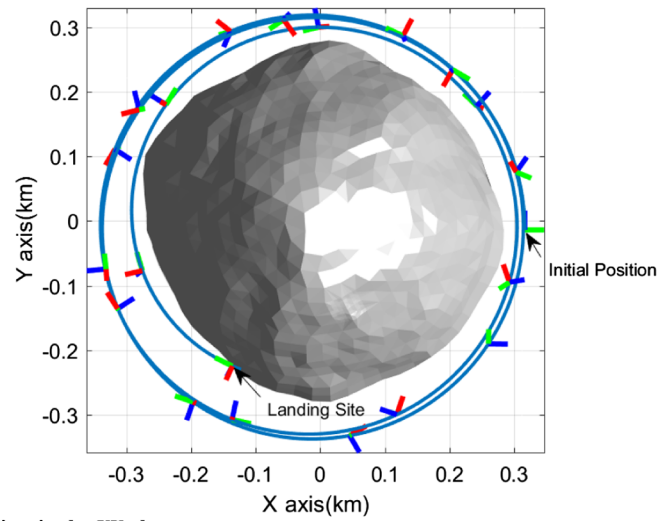
The initial attitude for the elliptic orbit is the same as in Table 5. The time interval between waypoints  $h_c$  is chosen as 500 s. The total time is 11 days. Figure 13 shows the orbits in the last day in the asteroid-fixed frame and the inertial frame, respectively. Compared with the natural motion, the orbit obtained using the control scheme in Sec. III is much closer to the reference trajectory. The maximum position error is about 7 m, as shown in Fig. 13c. Although the error slowly increases due to the limited control ability provided by the gravitational orbit–attitude coupling, it can reduce the frequency of orbit correction, which in turns saves fuel and prolongs the mission duration.

### C. Discussion

The preceding simulations show that the polyhedron model of the asteroid and the distributed point-mass model can better reflect the coupled orbit–attitude motion of the spacecraft in the vicinity of an irregular-shaped asteroid. They can provide more accurate analyses for couple trajectory design. Due to the gravitational orbit–attitude coupling, the rigid-body spacecraft trajectory will deviate from the point-mass reference trajectory. The trajectory tracking scheme given here, with only attitude control, can be used for the rigid-body trajectory design in small-body exploration missions. By using the gravitational orbit–attitude coupling itself, the spacecraft can track a desired point-mass landing trajectory without thrust control. This is due to the fact that the gravitational orbit–attitude coupling effect leading to the orbital position error between the point-mass and rigid body trajectories is of the same order of magnitude as the amount of force that can be produced from this coupling. For the elliptic orbit, the spacecraft can maintain near the reference orbit in several days. The same approach can be employed to track other desired trajectories, which require a similar amount of control effort. Besides, the attitude actuation is often regenerative. Therefore, the proposed tracking scheme is more fuel efficient than the direct translational control. It can also provide a backup control scheme when thruster failure happens. Although the asteroid shown in this simulation is a major-axis spinner, the tracking scheme given here can also be applied to a tumbling asteroid. This is because the full dynamics considered in designing the control law has no restriction on the angular velocity  $\Omega$ . The performance of the tracking scheme is closely related to the controllability analysis, for which the relation with various orbital elements and different shapes of asteroids will be a direction for future studies.

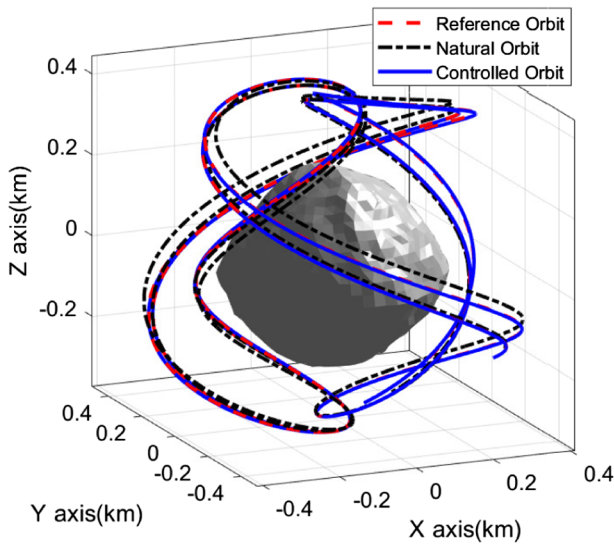


a) Three dimensional

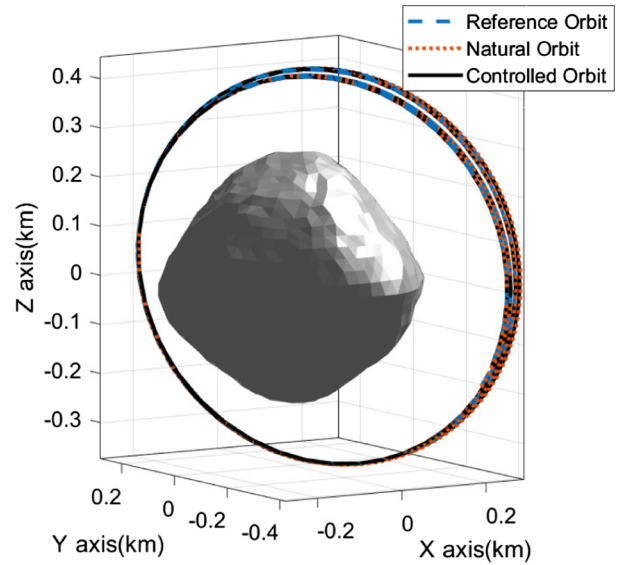


b) Project in the XY plane

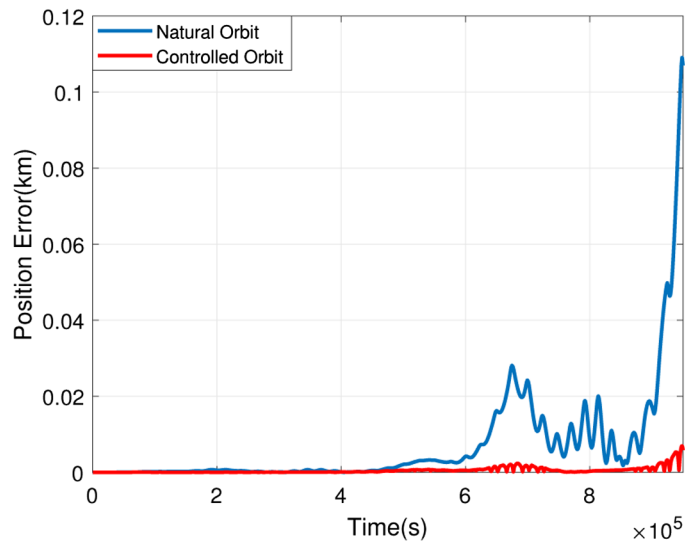
Fig. 12 Controlled landing trajectory in the inertial frame.



a) Tracking elliptic orbit in the asteroid-fixed frame



b) Tracking elliptic orbit in the inertial frame



c) Position error for the controlled elliptic orbit

Fig. 13 Controlled elliptic trajectory and position error.

## V. Conclusions

In this paper, a trajectory tracking scheme for rigid bodies with only attitude control is proposed for small-body missions using gravitational orbit–attitude coupling. The effect of gravitational orbit–attitude coupling is investigated based on a polyhedron model of the small body and a distributed point-mass model of the spacecraft, which shows higher accuracy than the spherical harmonic gravity model. The trajectory tracking method uses only an attitude control system, but no thrust control force input is applied to the spacecraft. The attitude of the spacecraft is controlled to generate a perturbation force induced by the gravitational orbit–attitude coupling, which is close to the designed virtual control thrust. This force drives the trajectory of the spacecraft to track a series of waypoints on a reference trajectory that is designed based on a point-mass trajectory. Simulation results show that the proposed tracking scheme can decrease the position trajectory error using the coupling effect without employing any translational control. It increases the landing accuracy to 0.3 m and keeps the tracking error less than 7 m over a period of 11 days. The tracking method does not require orbit control, therefore saving on fuel consumption. It also provides a redundant control scheme that can be used in the event of thruster failures. The approach outlined here can provide a reference for onboard control in future small-body missions.

## Acknowledgments

The first and fourth authors were supported by the National Natural Science Foundation of China (grant nos. 11572038 and 11772050), the Chang Jiang Scholars Program, and the Discipline Innovative Engineering Plan (111 Project). The second and third authors were supported in this research by the Syracuse University College of Engineering and Computer Science.

## References

- [1] Voosen, P., “NASA to Launch Asteroid-Sampling Mission,” *Science*, Vol. 353, No. 6303, 2016, pp. 974–975.  
doi:10.1126/science.353.6303.974
- [2] Miller, J. K., Konopliv, A., Antreasian, P., Bordi, J., Chesley, S., Helfrich, C., Owen, W., Wang, T., Williams, B., and Yeomans, D., et al., “Determination of Shape, Gravity, and Rotational State of Asteroid 433 Eros,” *Icarus*, Vol. 155, No. 1, 2002, pp. 3–17.  
doi:10.1006/icar.2001.6753
- [3] Saito, J., Miyamoto, H., Nakamura, R., Ishiguro, M., Michikami, T., Nakamura, A., Demura, H., Sasaki, S., Hirata, N., and Honda, C., et al., “Detailed Images of Asteroid 25143 Itokawa from Hayabusa,” *Science*, Vol. 312, No. 5778, 2006, pp. 1341–1344.  
doi:10.1126/science.1125722
- [4] Accomazzo, A., Ferri, P., Lodiot, S., Pellon-Bailon, J.-L., Hubault, A., Porta, R., Urbanek, J., Kay, R., Eiblmaier, M., and Francisco, T., “Rosetta Operations at the Comet,” *Acta Astronautica*, Vol. 115, No. 10, 2015, pp. 434–441.  
doi:10.1016/j.actaastro.2015.06.009
- [5] Witte, L., Roll, R., Biele, J., Ulamec, S., and Jurado, E., “Rosetta Lander Philae–Landing Performance and Touchdown Safety Assessment,” *Acta Astronautica*, Vol. 125, 2016, pp. 149–160.  
doi:10.1016/j.actaastro.2016.02.001
- [6] Li, X., Qiao, D., and Cui, P., “The Equilibria and Periodic Orbits Around a Dumbbell-Shaped Body,” *Astrophysics and Space Science*, Vol. 348, No. 2, 2013, pp. 417–426.  
doi:10.1007/s10509-013-1592-1
- [7] Jiang, Y., Baoyin, H., Li, J., and Li, H., “Orbits and Manifolds near the Equilibrium Points Around a Rotating Asteroid,” *Astrophysics and Space Science*, Vol. 349, No. 1, 2014, pp. 83–106.  
doi:10.1007/s10509-013-1618-8
- [8] Wang, X., Jiang, Y., and Gong, S., “Analysis of the Potential Field and Equilibrium Points of Irregular-Shaped Minor Celestial Bodies,” *Astrophysics and Space Science*, Vol. 353, No. 1, 2014, pp. 105–121.  
doi:10.1007/s10509-014-2022-8
- [9] Li, X., Qiao, D., and Barucci, M. A., “Analysis of Equilibria in the Doubly Synchronous Binary Asteroid Systems Concerned with Non-Spherical Shape,” *Astrodynamics*, Vol. 2, No. 2, June 2018, pp. 133–146  
doi:10.1007/s42064-017-0016-3
- [10] Scheeres, D. J., Ostro, S. J., Hudson, R. S., DeJong, E. M., and Suzuki, S., “Dynamics of Orbits Close to Asteroid 4179 Toutatis,” *Icarus*, Vol. 132, No. 1, 1998, pp. 53–79.  
doi:10.1006/icar.1997.5870
- [11] Yu, Y., and Baoyin, H., “Generating Families of 3D Periodic Orbits About Asteroids,” *Monthly Notices of the Royal Astronomical Society*, Vol. 427, No. 1, 2012, pp. 872–881.  
doi:10.1111/(ISSN)1365-2966
- [12] Scheeres, D. J., *Orbital Motion in Strongly Perturbed Environments: Applications to Asteroid, Comet and Planetary Satellite Orbits*, Springer, New York, 2016, p. 194.  
doi:10.1007/978-3-642-03256-1
- [13] Broschart, S. B., Scheeres, D. J., and Villac, B. F., “New Families of Multi-Revolution Terminator Orbits Near Small Bodies,” *Advances in the Astronautical Sciences*, Vol. 135, No. 3, 2009, pp. 1685–1702.
- [14] Scheeres, D., “Orbital Mechanics About Small Bodies,” *Acta Astronautica*, Vol. 72, No. 3, 2012, pp. 1–14.  
doi:10.1016/j.actaastro.2011.10.021
- [15] Broschart, S. B., and Scheeres, D. J., “Control of Hovering Spacecraft Near Small Bodies: Application to Asteroid 25143 Itokawa,” *Journal of Guidance, Control, and Dynamics*, Vol. 28, No. 2, 2005, pp. 343–354.  
doi:10.2514/1.3890
- [16] Nazari, M., Wauson, R., Critz, T., Butcher, E. A., and Scheeres, D. J., “Observer-Based Body-Frame Hovering Control over a Tumbling Asteroid,” *Acta Astronautica*, Vol. 102, No. 11, 2014, pp. 124–139.  
doi:10.1016/j.actaastro.2014.05.016
- [17] Furfaro, R., Cersosimo, D., and Wibben, D. R., “Asteroid Precision Landing via Multiple Sliding Surfaces Guidance Techniques,” *Journal of Guidance, Control, and Dynamics*, Vol. 36, No. 4, 2013, pp. 1075–1092.  
doi:10.2514/1.58246
- [18] Moran, J. P., “Effects of Plane Librations on the Orbital Motion of a Dumbbell Satellite,” *ARS Journal*, Vol. 31, No. 8, 1961, pp. 1089–1096.  
doi:10.2514/8.5724
- [19] Sincarsin, G., and Hughes, P., “Gravitational Orbit-Attitude Coupling for Very Large Spacecraft,” *Celestial Mechanics and Dynamical Astronomy*, Vol. 31, No. 2, 1983, pp. 143–161.  
doi:10.1007/BF01686816
- [20] Wang, Y., and Xu, S., “Relative Equilibria of Full Dynamics of a Rigid Body with Gravitational Orbit-Attitude Coupling in a Uniformly Rotating Second Degree and Order Gravity Field,” *Astrophysics and Space Science*, Vol. 354, No. 2, 2014, pp. 339–353.  
doi:10.1007/s10509-014-2077-6
- [21] Lian, K.-Y., Wang, L.-S., and Fu, L.-C., “Controllability of Spacecraft Systems in a Central Gravitational Field,” *IEEE Transactions on Automatic Control*, Vol. 39, No. 12, 1994, pp. 2426–2441.  
doi:10.1109/9.362852
- [22] Sanyal, A. K., *Dynamics and Control of Multibody Systems in Central Gravity*, Univ. of Michigan, Ann Arbor, MI, 2004, pp. 6–10.
- [23] Fahnestock, E. G., and Scheeres, D. J., “Dynamical Characterization and Stabilization of Large Gravity-Tractor Designs,” *Journal of Guidance, Control, and Dynamics*, Vol. 31, No. 3, 2008, pp. 501–521.  
doi:10.2514/1.32554
- [24] Wang, Y., and Xu, S., “Gravitational Orbit-Rotation Coupling of a Rigid Satellite Around a Spheroid Planet,” *Journal of Aerospace Engineering*, Vol. 27, No. 1, 2014, pp. 140–150.  
doi:10.1061/(ASCE)AS.1943-5525.0000222
- [25] Misra, G., Izadi, M., Sanyal, A., and Scheeres, D., “Coupled Orbit-Attitude Dynamics and Relative State Estimation of Spacecraft near Small Solar System Bodies,” *Advances in Space Research*, Vol. 57, No. 8, 2016, pp. 1747–1761.  
doi:10.1016/j.asr.2015.05.023
- [26] Wang, Y., and Xu, S., “Orbital Dynamics and Equilibrium Points Around an Asteroid with Gravitational Orbit-Attitude Coupling Perturbation,” *Celestial Mechanics and Dynamical Astronomy*, Vol. 125, No. 3, 2016, pp. 265–285.  
doi:10.1007/s10569-015-9655-y
- [27] Kikuchi, S., Howell, K. C., Tsuda, Y., and Kawaguchi, J., “Orbit-Attitude Coupled Motion Around Small Bodies: Sun-Synchronous Orbits with Sun-Tracking Attitude Motion,” *Acta Astronautica*, Vol. 140, No. 11, 2017, pp. 34–48.  
doi:10.1016/j.actaastro.2017.07.043
- [28] Wang, Y., and Xu, S., “Body-Fixed Orbit-Attitude Hovering Control over an Asteroid Using Non-Canonical Hamiltonian Structure,” *Acta Astronautica*, Vol. 117, No. 12, 2015, pp. 450–468.  
doi:10.1016/j.actaastro.2015.09.006
- [29] Lee, D., Sanyal, A. K., Butcher, E. A., and Scheeres, D. J., “Finite-Time Control for Spacecraft Body-Fixed Hovering over an Asteroid,” *IEEE Transactions on Aerospace and Electronic Systems*, Vol. 51, No. 1,

- 2015, pp. 506–520.  
doi:10.1109/TAES.2014.140197
- [30] Misra, G., Sanyal, A., and Samiei, E., “Asteroid Landing Guidance Design in the Framework of Coupled Orbit-Attitude Spacecraft Dynamics,” *25th AAS/AIAA Spaceflight Mechanics Meeting, Advances in the Astronautical Sciences*, AAS, Springfield, NJ, Vol. 155, No. 2, Jan. 2015, pp. 1969–1980.
- [31] Kulamani, S., Takami, K., and Lee, T., “Geometric Control for Autonomous Landing on Asteroid Itokawa Using Visual Localization,” *AAS Astrodynamics Specialist Conference, Advances in the Astronautical Sciences*, AAS, Springfield, NJ, Vol. 162, No. 3, Aug. 2017, pp. 1987–2001.
- [32] Viswanathan, S. P., Sanyal, A. K., and Misra, G., “Controllability Analysis of Spacecraft with only Attitude Actuation Near Small Solar System Bodies,” *IFAC-PapersOnLine*, Vol. 49, No. 18, 2016, pp. 648–653.  
doi:10.1016/j.ifacol.2016.10.239
- [33] Hu, X., and Jekeli, C., “A Numerical Comparison of Spherical, Spheroidal and Ellipsoidal Harmonic Gravitational Field Models for Small Non-Spherical Bodies: Examples for the Martian Moons,” *Journal of Geodesy*, Vol. 89, No. 2, 2015, pp. 159–177.  
doi:10.1007/s00190-014-0769-x
- [34] Hechler, M., “ROSETTA Mission Design,” *Advances in Space Research*, Vol. 19, No. 1, 1997, pp. 127–136.  
doi:10.1016/S0273-1177(96)00125-1
- [35] Beshore, E., Sutter, B., Mink, R., Lauretta, D., Moreau, M., Boynton, W., Dworkin, J., Everett, D., Shinohara, C., and Gal-Edd, J., “The OSIRIS-REx Asteroid Sample Return Mission,” *2015 IEEE Aerospace Conference*, IEEE Publ., Piscataway, NJ, 2015, pp. 1–14.  
doi:10.1109/AERO.2015.7118989
- [36] Bloch, A., Baillieul, J., Crouch, P., Marsden, J. E., Zenkov, D., Krishnaprasad, P. S., and Murray, R. M., *Nonholonomic Mechanics and Control*, Springer, New York, 2015, pp. 53–124.  
doi:10.1007/978-1-4939-3017-3
- [37] Werner, R. A., and Scheeres, D. J., “Exterior Gravitation of a Polyhedron Derived and Compared with Harmonic and Mascon Gravitation Representations of Asteroid 4769 Castalia,” *Celestial Mechanics and Dynamical Astronomy*, Vol. 65, No. 3, 1996, pp. 313–344.  
doi:10.1007/BF00053511
- [38] Fahnestock, E. G., and Scheeres, D. J., “Simulation of the Full Two Rigid Body Problem Using Polyhedral Mutual Potential and Potential Derivatives Approach,” *Celestial Mechanics and Dynamical Astronomy*, Vol. 96, No. 3, 2006, pp. 317–339.  
doi:10.1007/s10569-006-9045-6
- [39] Sanyal, A. K., Shen, J., McClamroch, N. H., and Bloch, A. M., “Stability and Stabilization of Relative Equilibria of Dumbbell Bodies in Central Gravity,” *Journal of Guidance, Control, and Dynamics*, Vol. 28, No. 5, 2005, pp. 833–842.  
doi:10.2514/1.10546
- [40] Lee, T., Leok, M., and McClamroch, N. H., “Lie Group Variational Integrators for the Full Body Problem in Orbital Mechanics,” *Celestial Mechanics and Dynamical Astronomy*, Vol. 98, No. 2, 2007, pp. 121–144.  
doi:10.1007/s10569-007-9073-x
- [41] Khalil, H. K., *Nonlinear Systems*, 3rd ed., Prentice-Hall, Upper Saddle River, NJ, 2001, pp. 323–325.
- [42] Bohn, J., and Sanyal, A. K., “Almost Global Finite-Time Stabilization of Rigid Body Attitude Dynamics Using Rotation Matrices,” *International Journal of Robust and Nonlinear Control*, Vol. 26, No. 9, 2016, pp. 2008–2022.  
doi:10.1002/rnc.v26.9
- [43] Viswanathan, S. P., Sanyal, A. K., and Samiei, E., “Integrated Guidance and Feedback Control of Underactuated Robotics System in SE(3),” *Journal of Intelligent and Robotic Systems*, Vol. 89, Nos. 1–2, Jan. 2018, pp. 251–263.  
doi:10.1007/s10846-017-0547-0
- [44] Nolan, M. C., Magri, C., Howell, E. S., Benner, L. A., Giorgini, J. D., Hergenrother, C. W., Hudson, R. S., Lauretta, D. S., Margot, J.-L., and Ostro, S. J., et al., “Shape Model and Surface Properties of the OSIRIS-REx Target Asteroid (101955) Bennu from Radar and Lightcurve Observations,” *Icarus*, Vol. 226, No. 1, 2013, pp. 629–640.  
doi:10.1016/j.icarus.2013.05.028
- [45] Werner, R. A., “Spherical Harmonic Coefficients for the Potential of a Constant-Density Polyhedron,” *Computers and Geosciences*, Vol. 23, No. 10, 1997, pp. 1071–1077.  
doi:10.1016/S0098-3004(97)00110-6
- [46] Chesley, S. R., et al., “Orbit and Bulk Density of the OSIRIS-REx Target Asteroid (101955) Bennu,” *Icarus*, Vol. 235, June 2014, pp. 5–22.  
doi:10.1016/j.icarus.2014.02.020
- [47] Herrera-Sucarrat, E., Palmer, P., and Roberts, R., “Asteroid Observation and Landing Trajectories Using Invariant Manifolds,” *Journal of Guidance, Control, and Dynamics*, Vol. 37, No. 3, 2014, pp. 907–920.  
doi:10.2514/1.59594